AGU ADVANCING EARTH AND SPACE SCIENCE

Water Resources Research

RESEARCH ARTICLE
10.1029/2020WR027792

Special Section:
Coastal Hydrology and Oceanography

Preventing Seawater Intrusion and Enhancing Safe Extraction Using Finite-Length, Impermeable Subsurface Barriers: 3D Analysis

Huiqiang Wu[1,2], Chunhui Lu[1,2], Jun Kong[1,3], and Adrian D. Werner[4]

[1]State Key Laboratory of Hydrology-Water Resources and Hydraulic Engineering, Hohai University, Nanjing, China, [2]Yangtze Institute for Conservation and Development, Hohai University, Nanjing, China, [3]Jiangsu Key Laboratory of Coast Ocean Resources Development and Environment Security, Hohai University, Nanjing, China, [4]College of Science and Engineering, and National Centre for Groundwater Research and Training (NCGRT), Flinders University, Adelaide, South Australia, Australia

Abstract Subsurface physical barriers have been recognized as effective in mitigating seawater intrusion in coastal aquifers, although mainly 2D (cross-sectional) barrier effects have been considered. In this study, impermeable barriers with finite shore-parallel lengths are investigated through 3D numerical simulation, thereby extending previous analyses. Two scenarios are considered: (a) barrier-only and (b) barrier-well systems; and three available barrier types are analyzed and compared: (1) subsurface dam, (2) cutoff wall, and (3) fully penetrating barrier. Barrier location, length, and height are investigated, and barrier effectiveness is evaluated from seawater volumes, seawater wedge toe positions, and maximum safe pumping rates. In the barrier-only system, a better performance in preventing seawater intrusion was achieved by cutoff walls rather than subsurface dams. Finite-length subsurface dams may slightly enhance seawater extent along parts of the coastline that are beyond the dam's length. Cutoff walls performed best when located at relatively small distances from the coast in the barrier-only system, whereas with a well at 450 m from the shoreline, the subsurface dam located at a critical distance from the sea (i.e., 300 m in the current study) performed optimally (from the tested cases) and was superior to cutoff walls in terms of the maximum safe pumping rate. A fully penetrating barrier outperformed cutoff walls and subsurface dams, as expected. Our investigation indicates that subsurface barrier design should consider the effect of the shore-parallel length, because barrier benefits may otherwise be significantly overestimated.

Key Points:
- Partially/fully penetrating impermeable barrier of finite-length analyzed in 3D coastal aquifer, with/without pumping well
- Subsurface dams reduced less seawater wedge volume than cutoff walls due to slightly enhanced seawater extent beyond the dam length
- Subsurface dams allowed larger maximum safe pumping rates than cutoff walls

Supporting Information:
- Supporting Information S1

Correspondence to:
C. Lu,
clu@hhu.edu.cn

Citation:
Wu, H., Lu, C., Kong, J., & Werner, A. D. (2020). Preventing seawater intrusion and enhancing safe extraction using finite-length, impermeable subsurface barriers: 3D analysis. *Water Resources Research*, *56*, e2020WR027792. https://doi.org/10.1029/2020WR027792

Received 23 APR 2020
Accepted 30 OCT 2020
Accepted article online 3 NOV 2020

1. Introduction

The fresh groundwater stored in coastal aquifers is relied upon throughout the globe, particularly where increasing populations are placing considerable stress on available fresh surface water resources (Michael et al., 2017). However, groundwater withdrawal from a coastal aquifer can disrupt the natural equilibrium between freshwater and seawater, resulting in landward invasion of saline groundwater and leading to the well-known seawater intrusion phenomena (Werner et al., 2013). Seawater intrusion can consequently threaten environmental assets, water supplies and coastal infrastructure, thereby justifying engineering solutions to mitigate or prevent its occurrence (Bear et al., 1999; Werner, 2010).

Various measures to control seawater intrusion have been introduced in recent decades. For example, optimization methods have been used to address various practical questions related to pumping operation, well placement, and the design of artificial recharge schemes (Ataie-Ashtiani & Ketabchi, 2011; Cheng et al., 2000; Mantoglou, 2003). Methods for exploiting fresh groundwater underlain by saltwater include the application of horizontal wells, skimming wells, and surface drains, which are simple and effective engineering measures to limit the upconing of saltwater (Custodio, 1987; Post et al., 2018). Other engineering strategies for maximizing the extraction of freshwater in coastal settings include the use of recharge wells or infiltration ponds to create hydraulic barriers (Dror et al., 2004; Lu et al., 2017; Mahesha, 1996b, 1996c; Masciopinto, 2013), the extraction of saltwater to reduce the saltwater volume and impose negative hydraulic barriers (Ebeling et al., 2019; Mahesha, 1996a), the injection of compressed air to reduce hydraulic conductivity (Dror et al., 2004; Sun & Semprich, 2013), and the construction of subsurface physical barriers (Abdoulhalik et al., 2017; Li et al., 2018; Pool & Carrera, 2010).

The construction of impermeable and semipermeable physical barriers to mitigate seawater intrusion has long been considered a potentially viable approach to enhancing the availability of coastal fresh groundwater (Anwar, 1983; Oude Essink, 2001; Werner et al., 2013). Subsurface barriers can be subdivided into three types, depending on the vertical penetration of the wall into the aquifer: (a) a "subsurface dam" is in contact with the aquifer base, with groundwater discharge possible above the barrier crest; (b) a "cutoff wall" is embedded into the upper part of the aquifer, allowing discharge to occur below the barrier; and (c) a "fully penetrating barrier" is intended to limit flow throughout the entire aquifer depth. All three barrier types can be designed to be impermeable or semipermeable.

Subsurface dams (i.e., type a) have been successfully applied to Japanese coastal aquifers to prevent seawater intrusion and increase fresh groundwater storage (Japan Green Resources Agency, 2004). In their field cases, seven subsurface dams were constructed to prevent seawater intrusion, where the lengths of dams are in the range of 74–550 m (except for a particularly long one, which is 2,432 m), the heights of dams are in the range of 13–86 m, and the widths of dams are in the range of 0.5–3 m (Japan Green Resources Agency, 2004).

Analyses of the effectiveness of subsurface dam designs in coastal aquifers have been undertaken presuming these to be impermeable and primarily using 2D conceptualizations and numerical models (i.e., using a cross-sectional representation of the aquifer). For example, Luyun et al. (2009) demonstrated through 2D laboratory experiments and numerical simulations that when the subsurface dam height exceeds the height of the saltwater wedge (i.e., prior to dam construction) at the site of the proposed subsurface dam, dam installation will exclude and eliminate the saltwater wedge from the aquifer on the landward side of the dam. However, Chang et al. (2019), based on the results of their 2D laboratory tests and numerical simulation, proposed that subsurface dam heights slightly lower than the saltwater wedge height (at the proposed dam location) can eliminate the saltwater wedge, thereby reducing construction costs.

Luyun et al. (2011) investigated the effectiveness of cutoff walls (i.e., type b) in controlling seawater intrusion using 2D laboratory-scale experiments and numerical simulations. They concluded that an impermeable cutoff wall that is deeper and closer to the coast is more efficient in mitigating seawater intrusion. Abdoulhalik and Ahmed (2017a, 2017b) extended the studies of Luyun et al. (2009, 2011) by considering a layered coastal aquifer, using both laboratory experiments and numerical modeling, again in 2D cross section. Their results showed that the ability of both subsurface dams and cutoff walls to inhibit seawater intrusion is highly dependent on the specific pattern of geological layering. They found, for example, that the existence of a naturally occurring low-hydraulic conductivity layer at the bottom of the aquifer led to smaller gains (in terms of changes in seawater extent in the aquifer) from the construction of either subsurface dams or cutoff walls.

Anwar (1983) developed a sharp-interface analytical solution for the freshwater-seawater distribution in an unconfined coastal aquifer with an embedded cutoff wall (i.e., type b). The analytical solution, validated experimentally using a vertical plane Hele-Shaw model, was found to apply to only a subset of coastal aquifer situations due to the Dupuit-Forchheimer approximation (i.e., the assumption of negligible vertical flow). The solution produced a reasonable match to coastal aquifers with small head drops across the barrier, which occur only when the barrier penetrates less than half the aquifer thickness; otherwise, the underlying assumptions are violated. Abdoulhalik et al. (2017) proposed a mixed barrier system, which combines an impermeable cutoff wall with a semipermeable subsurface dam. They investigated its effectiveness through 2D laboratory-scale experiments and numerical simulations, and found that the mixed-barrier system can outperform single-barrier systems (i.e., either a semipermeable subsurface dam or an impermeable cutoff wall) in terms of limiting seawater intrusion and incorporating barrier construction costs.

Previous investigations of the effectiveness of fully penetrating barriers (i.e., type c) in coastal aquifers have been conducted only through 2D experiments and numerical models, where fully penetrating barriers were presumed to be semipermeable (to avoid otherwise complete isolation of coastal aquifers from the sea in 2D analyses). For example, Sugio et al. (1987) demonstrated, based on the results of 2D laboratory experiments and numerical models, that a semipervious fully penetrating barrier can be effective in preventing seawater intrusion. Their site-specific analysis found that the subsurface barrier is able to delay seawater intrusion for about 2 months under the extreme conditions of total drought and the continuation of pumping. Mahesha (2009) used 2D numerical modeling, considering a sharp-interface approach, to analyze the effectiveness of a semipervious fully penetrating barrier in preventing/retarding seawater intrusion. The results

indicated that the barrier could significantly inhibit seawater intrusion that would arise from pumping. Mahesha and Lakshmikant (2014) investigated, also through a 2D numerical solution based on sharp-interface theory, the optimal locations for freshwater withdrawal in the presence of a semipervious fully penetrating barrier. The ideal positions of single, two, three, and four wells were identified. In the investigations of Mahesha (2009) and Mahesha and Lakshmikant (2014), the location of the semipervious fully penetrating barrier was fixed at the toe position of the seawater wedge (i.e., where the interface between freshwater and seawater meets the aquifer base) before barrier construction. The use of semipervious, rather than impervious, fully penetrating barriers is considered necessary to avoid excessive buildup of agricultural chemicals on the landward side of the barrier, although only 2D analyses of this issue have been undertaken (Mahesha & Lakshmikant, 2014; Sugio et al., 1987).

The aforementioned studies adopted 2D cross-sectional representations of subsurface barriers, whereby the barrier has an infinite length in the shore-parallel direction. While providing for efficient numerical simulation, this assumption may be invalid in practice due to cost constraints and construction limitations. Investigation is needed of subsurface barrier performance considering practical limits to barrier length, requiring 3D analysis. Moreover, the 2D cross-sectional analysis precludes the evaluation of the radial flow fields induced by freshwater pumping, and rather, previous studies have mostly focused on the effect of subsurface barriers on the location of the interface toe in the absence of pumping.

Few investigations have explored the effect of physical barriers on enhancing the allowable rate of fresh groundwater extraction from coastal wells. Only Kaleris and Ziogas (2013) have investigated the effect of subsurface barriers (they considered impermeable cutoff walls) on seawater intrusion and the safe extraction rate (of drains and single wells) in a narrow confined aquifer using 3D numerical simulation. They found that cutoff walls create a stronger protective effect for shore-parallel drains (i.e., the usual representation of freshwater extraction in 2D cross-sectional studies) compared to the protection afforded to single wells. However, their analysis only considered cutoff walls that extended the entire aquifer width along the shoreline (i.e., the shore-parallel length of the cutoff wall was equal to the width of the aquifer), such that flow around the wall's edges was not considered. Kaleris and Ziogas (2013) highlighted the need to investigate further the application of barriers with partial coverage of the aquifer width (i.e., where the shore-parallel length of the cutoff wall is shorter than the width of the aquifer) in protecting groundwater abstraction. To date, the effect of finite-length subsurface barriers on the mitigation of seawater intrusion and the enhancement of safe pumping rates has not been assessed.

In this study, 3D numerical modeling is used to investigate the effect of finite-length subsurface barriers on both the extent of seawater in the aquifer and the allowable rate of pumping from a single well (in a fixed location; 450 m from the shoreline). Three different subsurface barrier designs (types a, b, and c, as described above) are considered. The effect of the subsurface barrier will be examined for both barrier-only and barrier-well systems. The barrier performance is determined with respect to the barrier type, length, height, and distance from the shoreline. The results of this study are expected to provide guidance on the design of finite-length subsurface barriers aimed at preventing seawater intrusion and increasing fresh groundwater availability.

2. Method

2.1. Conceptual Model

A 3D, hypothetical, confined coastal aquifer (Figure 1) was used as the model domain in this study, with dimensions: L (length) × W (width) × H (depth), assuming symmetry about a shore-perpendicular axis that passes through the middle of the barrier (i.e., in the y direction; Figure 1). Where pumping effects are considered, a fully penetrating extraction well is located at a distance D_w from the coastline that pumps groundwater from the aquifer at a rate Q_w. An impermeable barrier with geometry L_b (length) × T_b (thickness) × h_b (height) is placed parallel to the coast at a distance D_b from the coastline. The seaside is represented by a specified-head boundary condition of hydrostatic seawater heads (H_s) with constant salt concentration $C = 35$ kg/m^3, without considering fluctuations caused by tides and waves. The inland boundary is assigned a seaward uniform freshwater flux (q_f) with salt concentration $C = 0$ kg/m^3, representing influx from inland recharge areas that is unmodified by the installation of barriers or the pumping of wells within the model domain. Other boundaries are impermeable (i.e., no-flow). The origin of the x, y, and z axes is located at

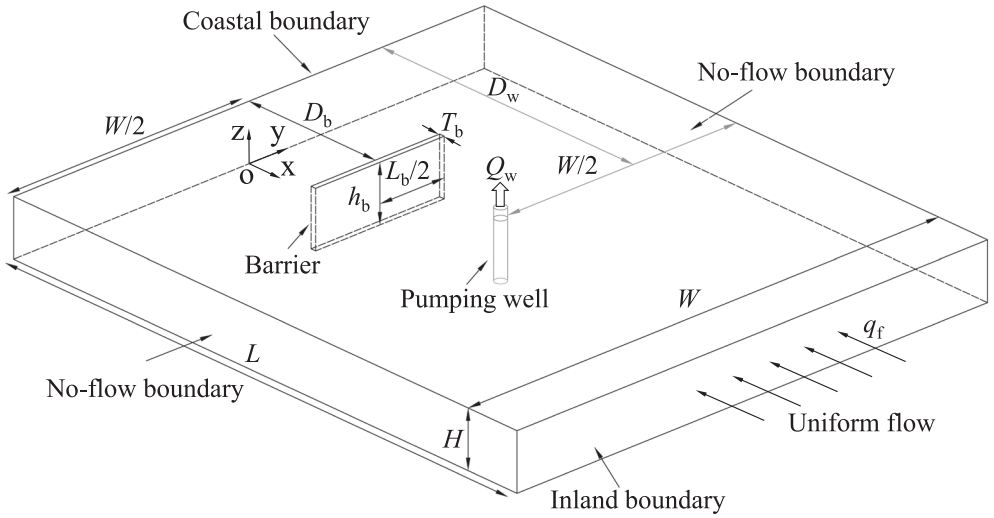

Figure 1. Conceptual model of a confined coastal aquifer containing a subsurface barrier and pumping well, showing boundary conditions and the aquifer, barrier, and well geometry.

the aquifer base (below the intersection of the coastline and the centerline of the domain width), whereby the x, y, and z axes are assigned to be horizontal, lateral, and vertical, respectively (Figure 1).

By varying the vertical position and penetration depth (h_b) of the barrier, three different barrier types are simulated, including the subsurface dam, cutoff wall, and fully penetrating barrier, as shown in Figure 2. All barriers are assumed to be impermeable.

2.2. Quantitative Indicators

To quantify the effectiveness of the barriers, volumes of seawater before and after barrier construction were calculated and compared. In the barrier-only system, we focus on the effectiveness of the barrier in excluding the seawater wedge on the landward side of the barrier (that existed prior to the barrier construction). Given seawater volumes on the landward side of the barrier before (V_{Ln}) and after (V_{Lc}) barrier construction, the

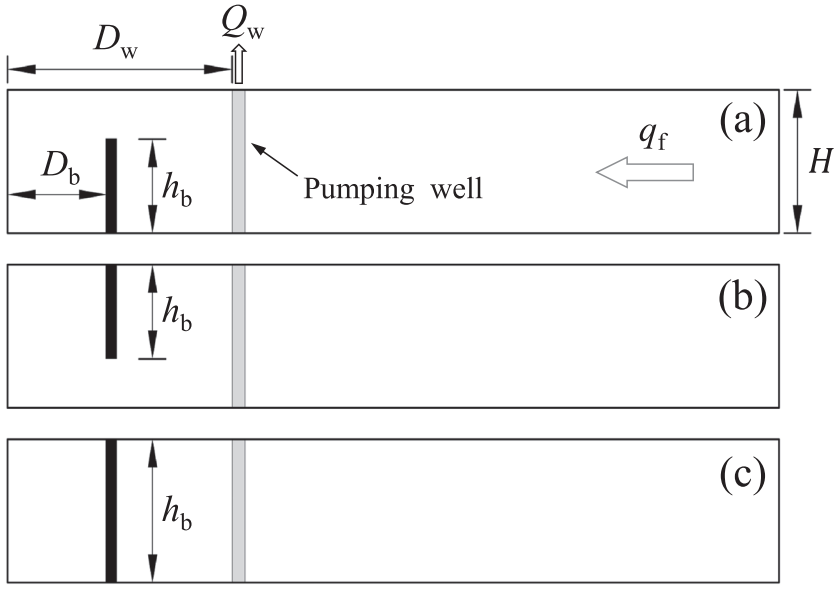

Figure 2. Cross-sectional views of the three types of impermeable subsurface barriers: (a) subsurface dam, (b) cutoff wall, and (c) fully penetrating barrier.

dimensionless change in seawater volume (on the landward side of the barrier) can be defined as: $\Delta V' = (V_{Ln} - V_{Lc})/V_n$, where V_n is the total volume of seawater in the aquifer before barrier construction. Obviously, greater $\Delta V'$ values indicate more effective barriers. Here, the volume of seawater (V) in the modeled domain was calculated by

$$V = \frac{\sum (\theta V_{i,j,k} C_{i,j,k})}{C_s} \quad (1)$$

where θ is the aquifer porosity, $V_{i,j,k}$ is the volume of model cell (i, j, k), $C_{i,j,k}$ is the salt concentration of model cell (i, j, k), C_s is the salt concentration of seawater, and $\sum$ represents the summation of model cells within the region of interest.

To characterize changes to the toe position of the seawater wedge resulting from barrier construction, the perpendicular distance from the shoreline to the toe was extracted from the model results at the center (i.e., at the model boundary; $y = 0$ m; Figure 1) and the edge (i.e., $y = L_b/2$) of the barrier, i.e., x_{Tc} and x_{Te}, respectively. The relative reduction of the toe position due to the barrier construction is given as

$$\Delta x_{Tc}' = (x_{Tn} - x_{Tc})/x_{Tn} \quad (2)$$

$$\Delta x_{Te}' = (x_{Tn} - x_{Te})/x_{Tn} \quad (3)$$

where x_{Tn} is the toe position before barrier construction, and relative changes in the toe position at the model center and the barrier edge are specified as $\Delta x_{Tc}'$ and $\Delta x_{Te}'$, respectively. Herein, the toe position of the saltwater wedge is defined as the point where the 25% salinity contour (i.e., salinity equal to 25% of seawater concentration) intersects the bottom of the aquifer, following the approach of Kaleris and Ziogas (2013). Linear interpolation between the salinities of adjacent cells was employed in calculating toe positions.

In a coastal aquifer, overpumping may result in saltwater entering the pumping well, leaving it unsuitable for drinking, or agricultural and industrial uses. We considered the maximum safe pumping rate as that causing the salt concentration of the pumped water under steady state to reach an allowable salt concentration limit (i.e., the maximum salt concentration allowed in the pumping well, denoted by C_m). In the study of Kaleris and Ziogas (2013), C_s and C_m were set to 35,700 and 500 ppm, respectively, producing $C_m/C_s = 0.014$. However, Pool and Carrera (2011) adopted $C_m/C_s = 0.001$ at the well as the salination threshold because the salinity at the well was found to be extremely sensitive to the pumping rate at that value. The same threshold (i.e., $C_m/C_s = 0.001$) is therefore adopted in the current study.

For barrier-well systems, maximum safe pumping rates were determined both before (Q_n) and after (Q_c) barrier construction. The relative increase in the maximum safe pumping rate attributable to barrier implementation is expressed as $\Delta Q' = (Q_c - Q_n)/Q_n$, where larger $\Delta Q'$ indicates improved well performance. Maximum safe pumping rates were determined by repeatedly running the model and modifying pumping through trial-and-error optimization. Maximum safe pumping was assumed to have been found when $0.00095 \leq C_m/C_s \leq 0.001$ through optimization. This range of C_m/C_s value was tested and was found to limit the error of $\Delta Q'$ to less than 0.2%.

2.3. Simulation Configurations

The numerical experiments to evaluate barrier effectiveness were conducted using SEAWAT-2000 (Guo & Langevin, 2002), which is a 3D finite-difference model that solves for variable-density flow and advective-dispersive solute transport. SEAWAT is one of the most commonly applied codes in seawater intrusion modeling and has been tested against several classical problems, including the Henry problem, the Elder problem, and the HYDROCOIN problem (Guo & Langevin, 2002; Langevin et al., 2003).

The scale of the studied area was selected to limit adverse influences of boundaries on freshwater-saltwater distributions (Lu et al., 2015). Preliminary simulations indicated that domain dimensions $L \times W \times H$ (see Figure 1) of 1,120 m × 2,250 m × 30 m were a reasonable trade-off that minimized both the computational load and boundary effects and allowed for a relatively fine grid resolution. The ratios $L/H = 37.3$ and $W/H = 75$ in the current investigation are larger than that of previous 3D studies of coastal

Table 1
Aquifer Properties and Solute Transport Parameters

Parameter	Value	Unit
Hydraulic conductivity (K)	10	m/d
Sea level (H_s)	35	m
Aquifer vertical thickness (H)	30	m
Freshwater discharge per unit width of coastline (q_f)	0.36	m^2/d
Freshwater density (ρ_f)	1,000	kg/m^3
Seawater density (ρ_s)	1,025	kg/m^3
Porosity (θ)	0.2	–
Molecular diffusion coefficient (D_m)	8.6×10^{-5}	m^2/d
Longitudinal dispersivity (α_L)	2.5	m
Transverse dispersivity (α_T)	0.25	m
Specific storage (S_s)	0.008	1/m

subsurface barriers and seawater intrusion (e.g., $W/H = 12$ and 18 in Kaleris and Ziogas (2013), where L/H was not mentioned; $L/H = 22$ and $W/H = 44$ in Pool and Carrera (2011)). Symmetry allows only half of the problem domain to be modeled (i.e., $W/2 = 1{,}125$ m).

In our investigation, the confined aquifer has uniform thickness (H) and is assumed to be horizontal, homogeneous and isotropic. The aquifer properties and solute transport parameters used in the simulations were adopted from previous seawater intrusion studies (e.g., K, D_m, and θ of Pool & Carrera, 2011; α_L and α_T of Kaleris & Ziogas, 2013; H and S_s of Lu & Werner, 2013; q_f of Lu et al., 2013) and are listed in Table 1. For the base case (i.e., no barrier and no pumping), the hydraulic head at the inland boundary produced by the model (recalling the specified-flux inland boundary condition) was 36.84 m (i.e., 6.84 m above the top of the confined aquifer).

Discretization of the model grid was adjusted considering the grid Péclet number (Pe_m). One-dimensional flow tests have indicated that when $Pe_m \leq 2$ (Zheng & Bennett, 2002), the finite-difference method is reasonably accurate and thus can be used with confidence. That is

$$Pe_m \approx \left(\frac{\Delta L}{\alpha_L}\right) \leq 2 \tag{4}$$

where ΔL is commonly taken as the cell size parallel to the groundwater flow direction. In a 3D model, Pe_m can be processed in a similar method to that suggested for 2D models by Zheng and Wang (1999). Specifically, the characteristic length ΔL is set to $\sqrt{\Delta x^2 + \Delta y^2 + \Delta z^2}$, where Δx, Δy, and Δz are grid spacings in the x, y, and z directions, respectively.

Based on the value of α_L given in Table 1, the discretization required to satisfy Equation 4 is $\Delta L < 5$ m. Accordingly, the 3D aquifer was discretized into 2,497,500 blocks, with constant cell sizes of $\Delta y = 2.5$ m and $\Delta z = 2$ m. The blocks had variable dimensions in the x direction, ranging from $\Delta x = 2.5$ m within areas expected to host the mixing zone (i.e., $x < 600$ m) to $\Delta x = 4$ m in inland regions where no mixing zone was anticipated (i.e., $x > 600$ m). The time step (Δt) used herein is 2.5 days, and the Courant number (C_r) is 1. This discretization scheme was examined in various preliminary test simulations, which produced head and salinity distributions that appeared to be free from numerical oscillations.

Simulations were undertaken using Intel i8 4.2-GHz processors with model run times ranging from 3 to >5 days in some cases. Ten observation wells (four parallel to the shoreline that are generally located on the landward side of the barrier and six perpendicular to the shoreline that are placed equidistantly between the coast and the extraction well) were added to the model to extract transient results aimed at monitoring whether steady-state conditions had been reached, i.e., to check when both concentrations and hydraulic heads reached time-invariant values. An observation well was placed at the well site to monitor whether the average salt concentration in the well column was constant (in time) and had reached the predefined threshold ($C_m/C_s = 0.001$). Simulation times that led to steady-state conditions ranged from 25 years (i.e., for the homogenous case without barrier and pumping) to approximately 200 years (i.e., for scenarios with barriers having the longest length, largest penetration depth and furthest distance from the coast).

The first scenarios of the current analysis involved a physical barrier without pumping (i.e., scenario a: barrier-only system). Here, to avoid boundary effects and to ensure a reasonable simulation time, the upper limit of L_b was set to 600 m. Luyun et al. (2011) suggested that saltwater intrusion can be effectively reduced if cutoff walls are constructed at distances from the coast that contained seawater prior to barrier construction. Therefore, the barrier was placed within 150 m from the coast, which is closer to the coast than the seawater toe position prior to barrier construction (i.e., $x_{Tn} = 184.3$ m). Impermeable barriers were simulated by inactivating model cells, effectively creating internal no-flow boundary conditions. The barrier height h_b was increased in 6-m increments from an initial value of 12 m to fully penetrating (i.e., 30 m). The barrier thickness, T_b, coincided with the cell size in the x direction (i.e., 2.5 m). Ranges of barrier geometric variables adopted in numerical simulations are listed in Table 2.

Table 2
Geometrical Variables of the Barrier

Geometrical variable	Model values (m)	Dimensionless values (−)
Barrier length (L_b)	400, 500, 600	0.89, 1.11, 1.33
Barrier location (D_b) tested in scenario (a)	0, 50, 100, 150	0, 0.11, 0.22, 0.33
Barrier location (D_b) tested in scenario (b)	0, 50, 100, 200, 300, 400	0, 0.11, 0.22, 0.44, 0.67, 0.89
Barrier height (h_b)	12, 18, 24, 30	0.4, 0.6, 0.8, 1.0

Conditions that arise from both a physical barrier and a pumping well (i.e., scenario b: barrier-well system) were also considered, using otherwise similar values for L_b and h_b as used in scenario (a), but with alternative values of D_b (see Table 2), which differed in scenario (b) to examine relationships between a wider range of D_b values and the maximum safe pumping rate (i.e., Q_c). Dimensionless parameters are introduced to facilitate the analysis of results, which are D_b', h_b', and L_b' (defined as D_b/D_w, D_b/D_w, and L_b/H, respectively). Values of dimensionless parameters are listed in Table 2.

3. Results

3.1. Scenario (a): Barrier-Only System

Figure 3 shows the 3D salt concentration distributions of barrier-only systems, including the cases without and with the addition of barriers, where $D_b' = 0.11$ and $L_b' = 1.11$. The seawater wedge intruded up to 184.3 m (i.e., x_{Tn}) from the coastline in the absence of a barrier (Figure 3a). Barrier construction subsequently reduced the saltwater wedge extent (Figures 3b–3d), as expected. Specifically, the subsurface dam, cutoff wall and fully penetrating barrier led to $x_{Tc} = 74.2$, 120.2, and 50.0 m, respectively. The fully penetrating barrier completely excluded saltwater (i.e., $x_{Tc} = D_b$) over almost the entire length of the barrier (Figure 3d), whereas partially penetrating barriers allowed seawater to extend landward of the barrier (Figures 3b and 3c). The fully penetrating barrier led to significant salinization on the seaward side of the barrier (Figure 3d), where extra seawater (about 23.7% by volume) was introduced relative to the unmodified scenario (i.e., Figure 3a). In contrast, there were slight decreases (about 5.8% and 1.0%) in the seawater volume on the seaward side of barriers in cases involving partially penetrating barriers (i.e., for subsurface dam and cutoff wall cases, respectively; Figures 3b and 3c).

Figure 4 shows salinity distributions within the shore-perpendicular cross section at the $y = 0$ m boundary. Results are included not only for the models represented in Figure 3 but also for alternative barrier height scenarios (i.e., $h_b' = 0.4$, 0.6, and 0.8). All barriers reduced the extent of saltwater, as expected. Cross-sectional views at the $y = 0$ m boundary of the 3D model show similar tendencies to those described in previous 2D investigations. That is, deeper penetration of the cutoff wall led to smaller saltwater wedges on the landward side of the cutoff wall (i.e., consider b1–b3 in Figure 4). A similar outcome was obtained for subsurface dams, whereby taller subsurface dams led to more shoreward wedge toes (i.e., a1–a4 in Figure 4),

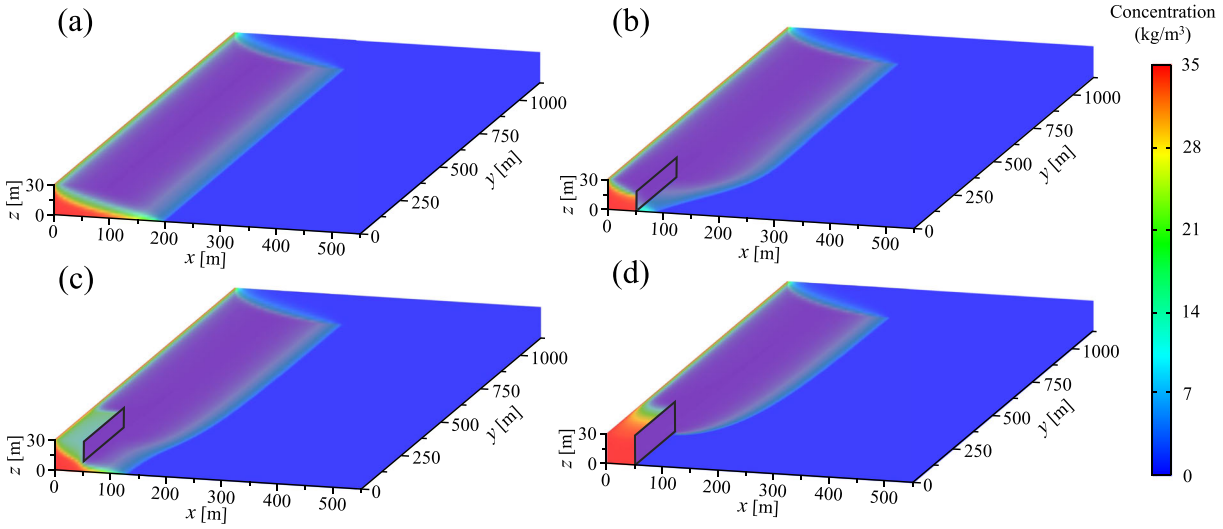

Figure 3. 3D, steady-state salinity distributions from simulations involving: (a) no barrier, (b) subsurface dam ($h_b' = 0.6$), (c) cutoff wall ($h_b' = 0.6$), and (d) fully penetrating barrier ($h_b' = 1.0$). Black parallelograms represent barrier geometries ($D_b' = 0.11$ and $L_b' = 1.11$).

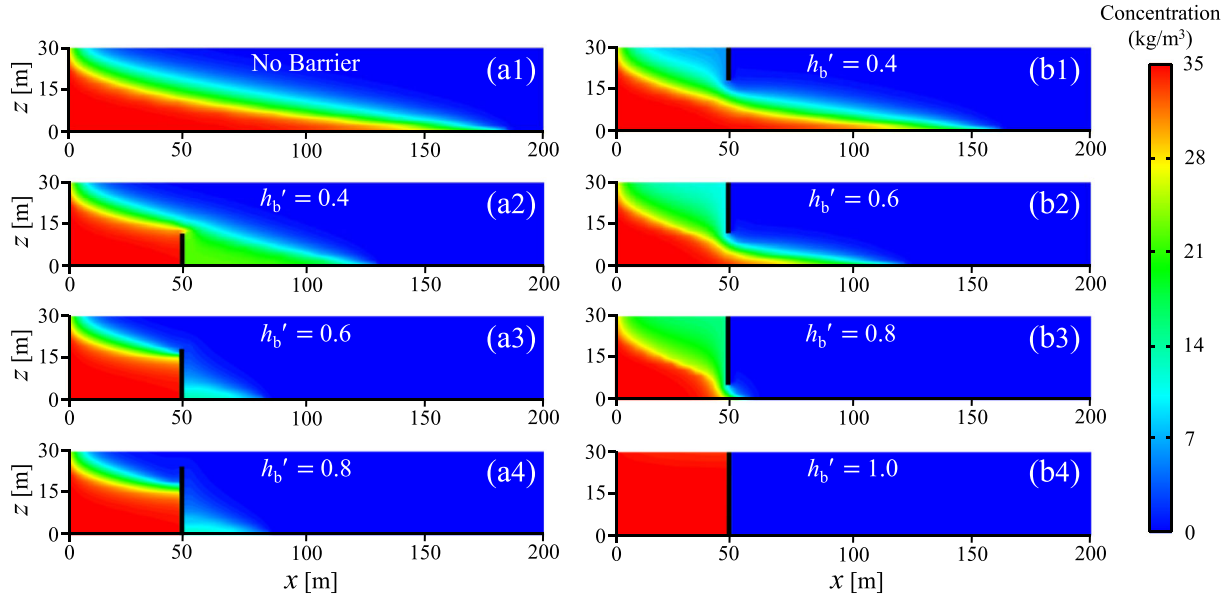

Figure 4. Salinity distributions in the shore-perpendicular cross section (at the $y = 0$ m boundary) with barriers (indicated by black vertical lines) of different heights, but all with $D_b' = 0.11$ and $L_b' = 1.11$.

although the occurrence of saltwater landward of the barrier in (a3) and (a4) of Figure 4 seems to be almost independent of the wall height.

2D numerical simulations that correspond with the aquifer scale, grid discretization, and parameters from 3D simulations adopted in our investigation were also conducted (Figure S1 in the supporting information). The 2D results in Figure S1 are consistent with the findings of Luyun et al. (2009), who found that residual saltwater can be completely excluded from the landward side of subsurface dams where the dam height exceeds the thickness of the prebarrier saltwater wedge (i.e., that existed prior to barrier construction) at that position, as mentioned above. However, the results of our 3D simulations show that saltwater may occur on the landward side of the barrier despite the height of the subsurface dam being higher than the prebarrier saltwater wedge. As shown in Figure 3b, saltwater landward of the subsurface dam was connected to the seawater wedge beyond the barrier coverage. In other words, seawater breached the barrier by passing around its lateral edge, although this resulted in predominantly highly diluted seawater landward of the surface dam (e.g., a2 in Figure 4). This effect is not captured by 2D numerical simulations (see Figure S1 and the results of Luyun et al. (2009)). In the 3D domain, exclusion of saltwater on the landward side of the barrier (e.g., at $y = 0$ m) occurred only in the case of a fully penetrating barrier (with $D_b' = 0.11$ and $L_b' = 1.11$; b4 in Figure 4). In that case, seaward freshwater flow was completely blocked by the barrier, causing groundwater to flow around the barrier (i.e., flow occurred parallel to the barrier axis on the landward side of the barrier), thereby flushing seawater from the landward side of the barrier.

The effect of the barrier height on the toe position of the seawater wedge (viewed in the *xy* plane) is illustrated in Figure 5, where $D_b' = 0.11$ and $L_b' = 1.11$. As expected, the toe is significantly shoreward where the barrier is located (solid lines, Figure 5) compared with the initial toe position (dashed lines, Figure 5). Barriers of greater height resulted in more shoreward toe locations, for both subsurface dams and cutoff walls, as expected, except that the toe positions for subsurface dam heights $h_b' = 0.6$ and 0.8 (red and green lines in Figure 5a) are almost coincident. This indicates that when h_b exceeds the prebarrier saltwater thickness at the subsurface dam location (i.e., 17.9 m), increasing h_b' may be inefficient (notwithstanding the seaward shift in the toe for $h_b' = 1.0$) in improving the subsurface dam effectiveness in terms of the toe shape along the shoreline.

As shown in Figure 5, the toe is furthest toward the sea at $y = 0$, while for $y > 0$, the toe is gradually further inland for subsurface dams and cutoff walls. For the fully penetrating barrier case, toe locations landward of

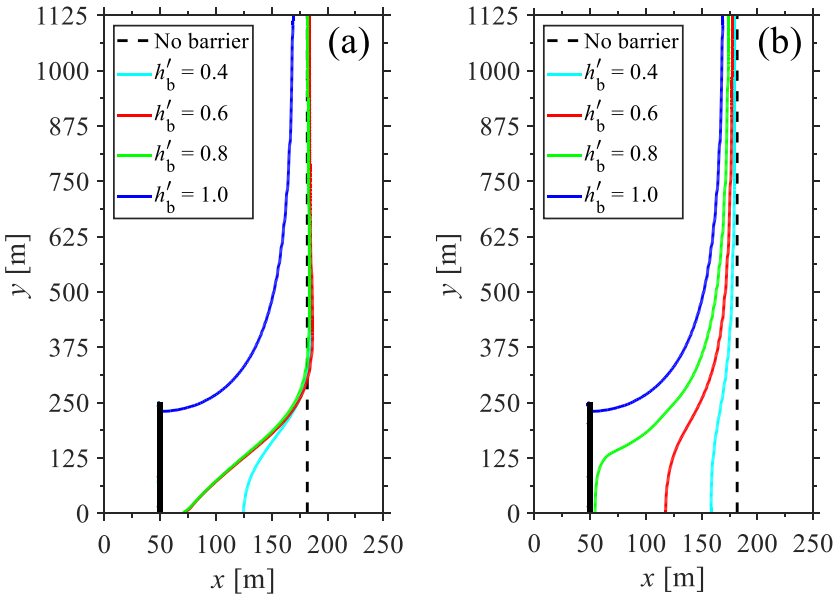

Figure 5. Effect of barrier height (h_b') on the saltwater wedge toe position for (a) subsurface dam and (b) cutoff wall cases, noting that all cases adopt $D_b' = 0.11$ and $L_b' = 1.11$. A fully penetrating barrier is represented by $h_b' = 1.0$. Black solid lines represent the barrier position.

the barrier were found only near the barrier's edge (i.e., $y > 230.4$ m). Figure 5a shows that subsurface dams may lead to toe positions that are landward, albeit slightly, of the prebarrier toe location in parts of the coastal aquifer that are beyond the extent of the barrier (i.e., $y > L_b/2$). That is, the red and green lines appear a little landward of the dashed line in Figure 5a. However, cutoff walls did not lead to the same phenomenon, as shown in Figure 5b.

The response of the seawater plume to the addition of subsurface dams and cutoff walls differed, as evidenced by the toe distributions in Figure 5. For example, cutoff walls reduced the seawater extent beyond the barrier's extent (i.e., $y > L_b/2$), whereas subsurface dams reduced the seawater extent only for the part of the coastline that contained the barrier (i.e., $y \leq L_b/2$). Differences between cutoff walls and subsurface dams were a consequence of dissimilar freshwater flow behavior between the two cases, as illustrated by velocity vectors given in Figure S2. For the subsurface dam case, freshwater mostly flows above the crest of the dam, whereby seawater wedge can penetrate unimpededly around the edge of the dam (Figures S2a and S2c). Nonetheless, the landward expansion of seawater around the center of the dam is highly limited by the seaward freshwater flow (which leads to the seaward dispersive flux above the crest; see Figure S2a). As observed in Figure S2c, the vectors of freshwater flow appear to shift toward the barrier center, which distracts the seaward freshwater flow on the shoreline beyond the dam coverage, i.e., resulting in the more landward toe position at $y > 375$ m for subsurface dam cases (i.e., red and green lines in Figure 5a) compared to the no-barrier case (i.e., black dashed line in Figure 5a). In the cutoff wall case, the barrier forces the freshwater to flow through the opening and thus effectively impede the lanward penetration of the saltwater (Figure S2b). The expansion of the saltwater from the edge is also limited by freshwater flow (of a nonnegligible component in the positive y direction, Figure S2d) at the base of the aquifer, i.e., where the toe of the seawater wedge is located.

For the fully penetrating barrier case, the velocity vectors adjacent to the landward side of the barrier are virtually parallel to the barrier axis (i.e., flowing in the positive y direction; see Figure S3). Differences in the toe distributions arising from finite-length subsurface dams and cutoff walls indicate that the barrier effectiveness needs to account for more than just the toe position change at the barrier center (i.e., $y = 0$ m), which is in effect the focus of previous analyses undertaken in 2D cross section.

Values of the sensitivities $\Delta V'$, $\Delta x_{Tc}'$ and $\Delta x_{Te}'$ for different h_b' and D_b' are presented in Figure 6 (for the cases with $L_b' = 1.11$). Figures 6a and 6b show that both cutoff walls and subsurface dams led to larger

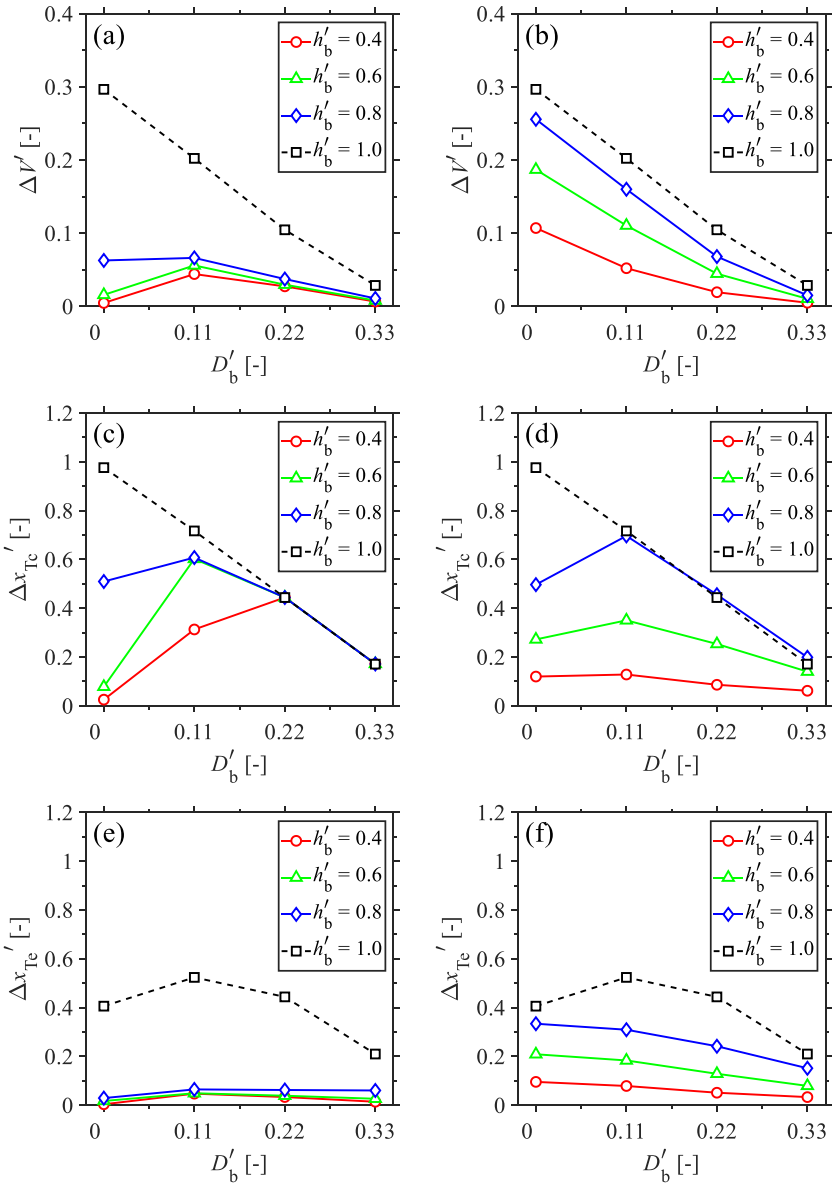

Figure 6. Values of sensitivity parameters $\Delta V'$, $\Delta x_{Tc}'$, and $\Delta x_{Te}'$ with differences in h_b' and D_b' (with $L_b' = 1.11$) for the cases: (a) subsurface dam, $\Delta V'$ versus D_b', (b) cutoff wall, $\Delta V'$ versus D_b', (c) subsurface dam, $\Delta x_{Tc}'$ versus D_b', (d) cutoff wall, $\Delta x_{Tc}'$ versus D_b', (e) subsurface dam, $\Delta x_{Te}'$ versus D_b', and (f) cutoff wall, $\Delta x_{Te}'$ versus D_b'. Black dashed lines represent fully penetrating barrier cases.

$\Delta V'$ values as h_b' increased, whereby the maximum $\Delta V'$ for a given D_b' was obtained for fully penetrating barriers (black dashed lines). Additionally, cutoff walls (Figure 6b) generally outperformed subsurface dams (Figure 6a). These trends are consistent with the salinity and toe location results illustrated in Figures 4 and 5. The ideal location (D_b'), in terms of seawater volume landward of the barrier, appears to be 0.11 for subsurface dams (Figure 6a), at least for the four D_b' values tested, whereas cutoff walls and fully penetrating barriers were ideally located at the shoreline ($D_b' = 0$; Figure 6b).

Figures 6a–6d (black dashed line) show that both $\Delta V'$ and $\Delta x_{Tc}'$ are approximately inversely related to D_b' for the fully penetrating barrier cases (in fact, $x_{Tc} = D_b$). That is, fully penetrating barriers performed optimally (in terms of $\Delta V'$ and $\Delta x_{Tc}'$) with D_b' equal to 0 (i.e., coincident with the shoreline). The fully penetrating barrier performed optimally in terms of $\Delta x_{Te}'$ when D_b' was 0.11 (Figure 6e), rather than the D_b' value of 0 for $\Delta V'$ and $\Delta x_{Tc}'$ given above. This result is attributed to the larger seawater wedge thickness (and

therefore saltwater head) on the seaward side of the fully penetrating barrier with $D_b' = 0$ compared to $D_b' = 0.11$. This forced more seawater around the wall's edge when it was placed at the shoreline, leading to a larger value of x_{Te}, which equates to a smaller value of $\Delta x_{Te}'$ (Equation 3).

Subsurface dams with higher walls (larger h_b') gave rise to toe positions that were more seaward (i.e., greater $\Delta x_{Tc}'$) with $D_b' = 0$ or 0.11 (Figure 6c). However, with $D_b' = 0.22$ or 0.33, subsurface dams of all h_b' values produced the same $\Delta x_{Tc}'$ as the fully penetrating barriers (i.e., due to $x_{Tc} = D_b$ in all cases). This arose because subsurface dams of all heights excluded seawater from the landward side of the wall at the $y = 0$ m boundary, at least up to the salinity used to define the toe (i.e., 25% of seawater salinity). For the cutoff wall cases, increasing h_b' (from 0.4 to 0.8) resulted in significant increases in $\Delta x_{Tc}'$ (Figure 6d) for all values of D_b'. Cutoff walls of $h_b' = 0.8$ produced $\Delta x_{Tc}'$ values similar to fully penetrating barriers for $0.11 \le D_b' \le 0.33$. In fact, with $D_b' = 0.22$ or 0.33, $\Delta x_{Tc}'$ was slightly larger than that from the corresponding fully penetrating barrier cases. This is because cutoff walls allow freshwater to flow through underlying openings, which resulted in $x_{Tc} < D_b$ in those cases and led to values of $\Delta x_{Tc}'$ larger than that of the fully penetrating barriers (for which $x_{Tc} = D_b$, as discussed above). Optimum subsurface dam and cutoff wall performances, in terms of $\Delta x_{Tc}'$, were obtained for the value of D_b' equal to 0.11, except for the subsurface dam case with $h_b' = 0.4$, for which $D_b' = 0.22$ produced the peak $\Delta x_{Tc}'$.

Low values of $\Delta x_{Te}'$ in Figure 6e show that subsurface dams were relatively ineffective in shifting the toe location seaward at the barrier edge (x_{Te}). This was largely unaffected by the subsurface dam height, such that increasing h_b' from 0.4 to 0.8 caused only small increases in $\Delta x_{Te}'$. Major differences in $\Delta x_{Te}'$ were obtained between subsurface dams and fully penetrating barriers (i.e., $h_b' = 1.0$). This arose because the subsurface dam allows seawater to penetrate around the dam edge (where freshwater mainly flows above the crest; Figure S2c), whereas the fully penetrating barrier blocks the freshwater flow in the y direction (at the barrier location), where the freshwater flow turns to the barrier edge (Figure S3), thereby effectively preventing landward seawater movement around the barrier edge (i.e., producing a large $\Delta x_{Te}'$). The ineffectiveness of subsurface dams in excluding saltwater at the barrier edge (i.e., $y = L_b/2$) was also apparent in Figure 5a. On the contrary, significant increases in $\Delta x_{Te}'$ were achieved as h_b' increased from 0.4 to 0.8 for the cutoff wall cases (Figure 6f). This is also apparent in Figure 5b. The fully penetrating barrier produced $\Delta x_{Te}'$ values larger than those from both subsurface dams and cutoff walls (Figures 6e and 6f), as expected.

Figure 7 shows the sensitivities of $\Delta V'$, $\Delta x_{Tc}'$, and $\Delta x_{Te}'$ to different L_b' and D_b', for the subsurface dam and the cutoff wall cases with $h_b' = 0.8$, and for fully penetrating barrier cases. As shown in Figures 7a–7c, all barrier types performed optimally with the largest L_b' (i.e., 1.33). Cutoff walls (Figure 7b) were superior to subsurface dams (Figure 7a) in terms of the value of $\Delta V'$, while fully penetrating barriers produced the largest $\Delta V'$ for a given L_b' and D_b' (Figure 7c). The optimal D_b' (i.e., leading to the peak $\Delta V'$) occurred at 0.11 for subsurface dam cases with $L_b' = 0.89$ and 1.11. However, with $L_b' = 1.33$, the subsurface dam placed at the shoreline ($D_b' = 0$) produced the maximum $\Delta V'$ (Figure 7a). Cutoff walls and fully penetrating barriers were ideally located (i.e., creating the peak $\Delta V'$) at the shoreline ($D_b' = 0$).

Figures 7d and 7e show that subsurface dams and cutoff walls of larger L_b' produced greater $\Delta x_{Tc}'$, with $D_b' = 0$ and 0.11. However, with $D_b' = 0.22$, the same $\Delta x_{Tc}'$ was obtained for all tested values of L_b' (due to $x_{Tc} = D_b$). This was also observed for fully penetrating barrier cases (Figure 7f), such that all tested values of L_b' led to the same $\Delta x_{Tc}'$ for a given D_b' (due to $x_{Tc} = D_b$). The ideal location, in terms of the tested D_b' values that producing largest $\Delta x_{Tc}'$, appeared to be 0.11 for both subsurface dam and cutoff wall cases (of all L_b' values tested), whereas the fully penetrating barrier performed optimally on the shoreline ($D_b' = 0$).

The values of $\Delta x_{Te}'$ for the subsurface dam case decreased, albeit slightly, as L_b' increased (Figure 7d). That is, shorter subsurface dams (i.e., smaller L_b') were marginally more effective in reducing the toe location at the barrier edge (x_{Te}). Conversely, longer cutoff walls (i.e., larger L_b') gave rise to a greater $\Delta x_{Te}'$ (Figure 7e). Increasing the value of L_b' also led to increasing $\Delta x_{Te}'$ for the fully penetrating barrier with $D_b' = 0$ and 0.11 (Figure 7f), whereas for $D_b' = 0.22$, $\Delta x_{Te}' = \Delta x_{Tc}'$ was obtained. That is, fully penetrating barriers placed at $D_b' = 0.22$ were able to completely exclude seawater from the landward side of the barrier over the entirety of the barrier-covered shoreline (i.e., 0 m $< y < L_b/2$), at least up to the predefined salinity of 25% of seawater.

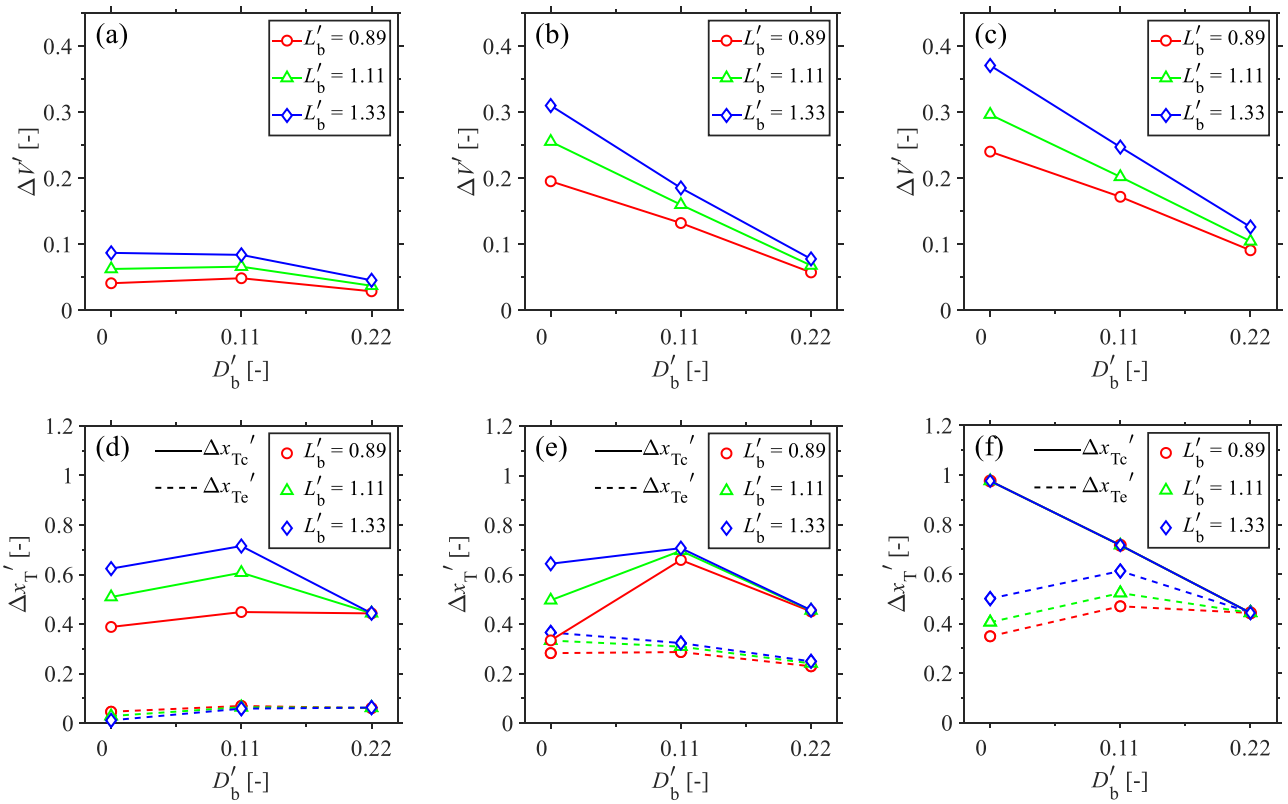

Figure 7. Sensitivity of $\Delta V'$, $\Delta x_{Tc}'$, and $\Delta x_{Te}'$ to L_b' and D_b': (a) subsurface dam, $\Delta V'$ versus D_b'; (b) cutoff wall, $\Delta V'$ versus D_b'; (c) fully penetrating barrier, $\Delta V'$ versus D_b'; (d) subsurface dam, $\Delta x_T'$ versus D_b'; (e) cutoff wall, $\Delta x_T'$ versus D_b'; and (f) fully penetrating barrier, $\Delta x_T'$ versus D_b', where $h_b' = 0.8$ and 1.0 for partially and fully penetrating barrier cases, respectively. Note that in (f), lines of $\Delta x_{Te}'$ versus D_b' for $L_b' = 0.89$, 1.11, and 1.33 (i.e., solid lines) coincide.

Furthermore, the sensitivities of $\Delta V'$, $\Delta x_{Tc}'$, and $\Delta x_{Te}'$ to different L_b' and D_b', for the subsurface dam and the cutoff wall cases with $h_b' = 0.4$ and 0.6, are also conducted, which, for the sake of brevity, is incorporated into Section S4.1 and Figure S10.

3.2. Scenario (b): Barrier-Well System

Figure 8 shows the 3D salt concentration distributions for barrier-well systems, including the cases without and with barriers (i.e., located at $D_b' = 0.67$ and of length $L_b' = 1.11$). The maximum safe pumping rates (i.e., Q_n and Q_c), for the wells in four cases (i.e., a–d) shown in Figure 8 were found to be 191.6, 202.0, 296.6, and 325.2 m^3/d, respectively. The modeling results show that pumping caused the seawater wedge to migrate toward the well in the form of a narrow tongue in the absence of a barrier and with the cutoff wall (Figures 8a and 8c). The tongue of seawater passing through the opening beneath the cutoff wall (Figure 8c) led to only a slight increase from Q_n = 191.6 m^3/d to Q_c = 202.0 m^3/d (i.e., with the addition of the cutoff wall). However, the subsurface dam and fully penetrating barriers created a build-up of seawater on the seaward side of those barriers due to restriction to the landward penetration (along the aquifer base) of seawater toward the well (Figures 8b and 8d). As a consequence, larger Q_c values were obtained for the subsurface dam and fully penetrating barrier cases (i.e., 296.6 and 325.2 m^3/d, respectively).

Figure 9 shows salinity distributions in the shore-perpendicular cross section at the y = 0 m boundary. Results are included not only for the barrier-well models represented in Figure 8 but also for alternative barrier location scenarios (i.e., $D_b' = 0$, 0.22, 0.44, 0.67, and 0.89). In each case, the well was pumping at the maximum safe pumping rate. All barriers led to $Q_c > Q_n$, as expected.

The modeling results show that subsurface dams produced increasing $\Delta Q'$ values as D_b' increased from 0 to 0.67 (Figures 9a–9d). However, the subsurface dam at $D_b' = 0.89$ resulted in a relatively low value of $\Delta Q'$ (Figure 9e). The performance of the subsurface dam is associated with the mechanisms of saltwater

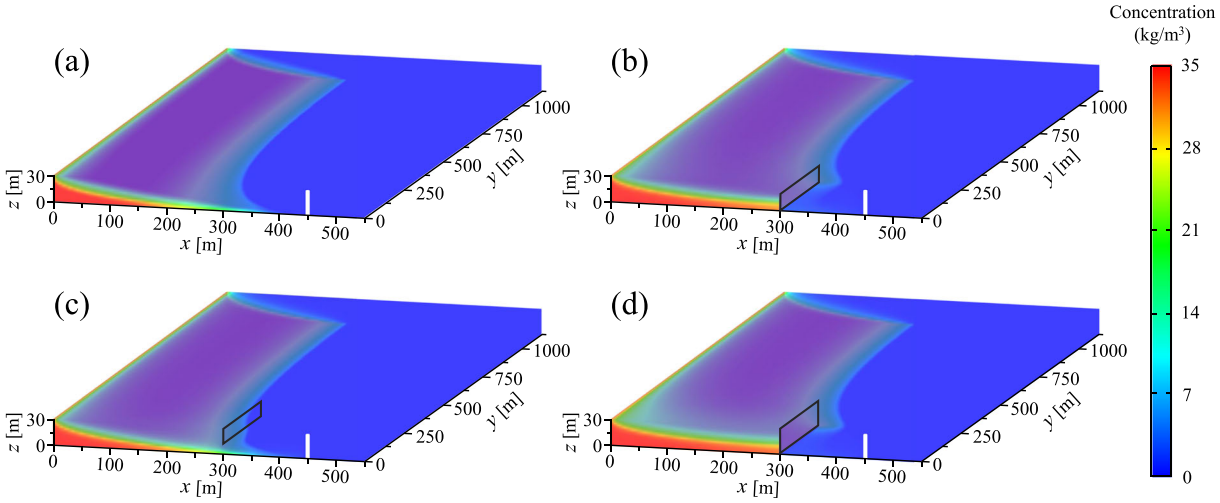

Figure 8. 3D, steady-state salinity distributions from simulations involving: (a) no barrier, (b) subsurface dam ($h_b' = 0.6$), (c) cutoff wall ($h_b' = 0.6$), and (d) fully penetrating barrier ($h_b' = 1.0$). The wells (indicated by the white columns) operate at the maximum safe pumping rates in all cases. Black parallelograms represent barrier geometries ($D_b' = 0.11$ and $L_b' = 1.11$).

landward movement, i.e., overtopping of the dam opening and bypassing around the barrier's vertical edge, under the action of maximum safe pumping. This is evident from the velocity vectors (at the $y = 0$ m cross section) and the salinity distributions (at the $y = 250$ m cross section; the edge of the barrier) shown in Figures S4 and S5, respectively.

Both saltwater overtopping at the $y = 0$ m boundary (Figure S4a) and saltwater bypassing the barrier's vertical edge (Figure S5a) were observed for the subsurface dam case with $D_b' = 0$, for which the lowest $\Delta Q'$ was obtained (Figure 9a). For the cases of $D_b' = 0.22$–0.67, freshwater discharge over the barrier repressed saltwater overtopping at the $y = 0$ m boundary (Figures S4b–S4d). Thus, saltwater movement around the barrier

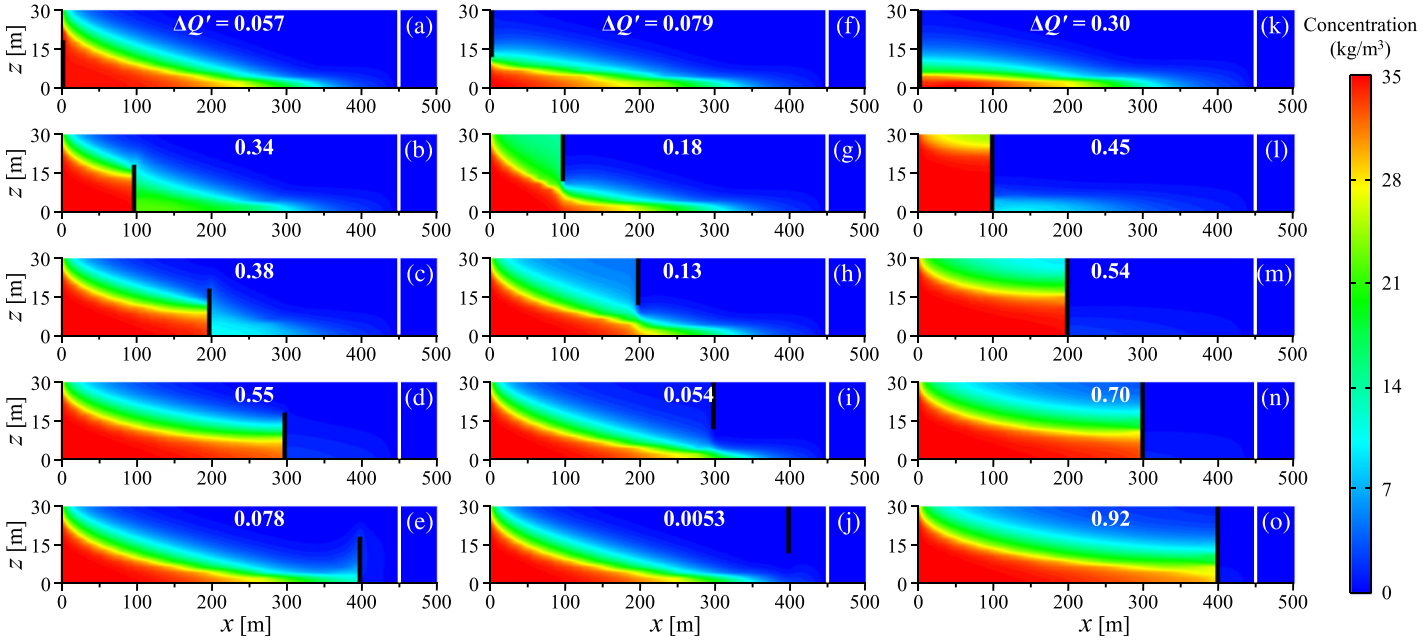

Figure 9. Salinity distributions within shore-perpendicular cross sections (i.e., at the $y = 0$ m boundary) with barriers (indicated by black vertical lines) of different D_b', but all barriers with $L_b' = 1.11$ and $h_b' = 0.6$ (i.e., for partially penetrating barriers; $h_b' = 1.0$ for fully penetrating barriers). Wells are represented by white vertical columns, and pumping occurs at maximum safe rates (Q_c) that are reflected by values of $\Delta Q'$ given in white writing at the top of each plot.

edge is the primary mechanism for well salinization with $D_b' = 0.22$–0.67, whereby at increasing distances from the shoreline, the depth of saltwater on the seaward side of the dam is reduced, and thereby the landward incursion of saltwater is increasingly limited to the barrier's vertical edge (Figures S5b–S5d). However, with $D_b' = 0.89$, saltwater overtopping was observed at the $y = 0$ m boundary and saltwater did not bypass the barrier's vertical edge (Figure S5e). This is attributable to the well-barrier proximity (Figure S4e), where the saltwater on the seaward side of the dam is directly impacted by the extraction well, leading to saltwater overtopping over the distance $y = 0.0$–56.1 m (see Figure S6). The lack of seawater movement around the edge of the dam and the observed saltwater overtopping in that case led to a relatively low value of $\Delta Q'$ (see Figure 9e).

Values of $\Delta Q'$ obtained for the cutoff wall cases were generally lower than those of subsurface dams, except for barriers at the shoreline ($D_b' = 0$), where the cutoff wall outperformed the subsurface dam in terms of the maximum safe pumping rate, although $\Delta Q'$ was low for both barrier types at $D_b' = 0$ (Figure 9). This can be attributed to the subsurface dam placed on the shoreline being submerged by the seawater wedge, thereby imposing little resistance to seawater incursion (see Figures 9a and S5a), whereas the cutoff wall at $D_b' = 0$ significantly lowered the seawater wedge (Figures 9f and S5f) leading to relatively high $\Delta Q'$. For the cases of $D_b' \geq 0.22$, the subsurface dam imposes greater resistance than the cutoff wall to seawater incursion, which tends to occur along the aquifer base (where the cutoff wall has an opening) due to density effects.

Figures 9f–9j show that the optimal cutoff wall location (in terms of the tested D_b' values that producing largest $\Delta Q'$) was 0.22. At locations of $D_b' = 0.89$, the cutoff wall was virtually ineffective ($\Delta Q'$ is lower than 0.01). It appears from velocity vector distributions (at the $y = 0$ m cross section; see Figure S4) that cutoff wall performance is related to the combined effect of the seaward freshwater flow (i.e., preventing the seawater wedge) and the pumping stresses (i.e., dragging the seawater wedge). Where the cutoff wall is closer to the coast (e.g., $D_b' \leq 0.67$), the barrier effectively exerts repulsion of the seawater wedge as a consequence of the seaward freshwater flow through the opening (Figures S4f–S4i), but otherwise, the wedge can pass below the wall relatively unimpeded under the actions of maximum safe pumping (e.g., $D_b' = 0.89$; Figure S4j). The addition of the wall at that location (i.e., $D_b' = 0.89$) diminishes the freshwater flow preventing the wedge (i.e., no vectors going downward through the opening to impede the intruding wedge in Figure S4j), resulting in a low value of $\Delta Q'$.

Figures 9k–9o show that fully penetrating barriers of greater D_b' led to larger$\Delta Q'$. In fully penetrating barrier cases, saltwater incursion occurs only by bypassing the vertical edge of the barrier. Shifting the barrier away from the shoreline created smaller depths of saltwater on the seaward side of the dam edge (see Figures S5k–S5o), thereby reducing saltwater bypass, leading to higher maximum safe pumping (i.e., larger $\Delta Q'$). Fully penetrating barriers achieved larger values of $\Delta Q'$ than partially penetrating cases ($h_b' = 0.6$) for every value of D_b' tested, as expected.

Figure 10 shows the sensitivity of $\Delta Q'$ to h_b' and D_b', with $L_b' = 1.11$. As shown in Figure 10a, relationships between $\Delta Q'$ and h_b', D_b', and L_b' are complex. For example, taller subsurface dams (larger h_b') produced greater values of $\Delta Q'$ with $D_b' = 0$, 0.67, and 0.89, whereas the largest $\Delta Q'$ was obtained with $h_b' = 0.6$, 0.6, and 0.4 when the barrier was located at $D_b' = 0.11$, 0.22, and 0.44, respectively. For all values of D_b' except $D_b' = 0$, fully penetrating barriers were more effective (higher $\Delta Q'$) than subsurface dams. For $D_b' = 0$, the subsurface dam of $h_b' = 0.8$ obtained a $\Delta Q'$ slightly larger than that of the fully penetrating barrier (Figure 10a). This occurs because, although the saline water can seep over the dam crest, the opening above the dam allows a great portion of the seaward freshwater flow to exclude saltwater (Figure S7a), thus depressing the penetration of the wedge driven by pumping stresses (Figure S7c). However, in the fully penetrating barrier case, the barrier blocks the freshwater flow over the crest (Figure S7b), where freshwater (on the shoreline that is beyond the barrier coverage) is attracted to flow around the edge of the barrier, rather than exerting resistance to the saltwater encroachment toward the extraction well. This is apparent from the velocity vectors and salinity distributions shown in Figure S7. Similarly, when the barrier was located at $D_b' = 0.44$, the dam with $h_b' = 0.4$ allows a greater portion of the seaward freshwater flow to exclude saltwater over the dam crest than a higher one, thereby producing a larger $\Delta Q'$.

Figure 10a indicates that the value of $\Delta Q'$ had an increasing trend as the subsurface dam was shifted from $D_b' = 0$–0.67 for a given h_b'. However, for $D_b' = 0.89$, relatively low values of $\Delta Q'$ were obtained compared to

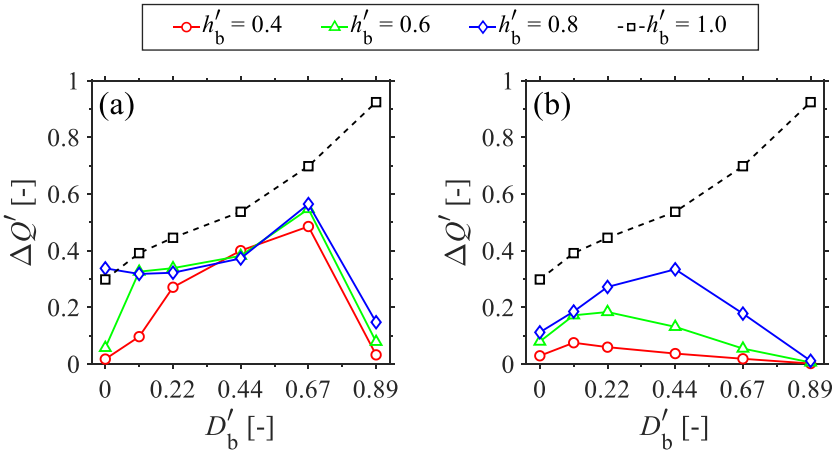

Figure 10. Sensitivity of $\Delta Q'$ to h_b' and D_b' ($L_b' = 1.11$) for the case of: (a) subsurface dam and (b) cutoff wall. Black dashed lines represent the results of the fully penetrating barrier cases.

the subsurface dam cases of $0.11 \le D_b' \le 0.67$. The optimal D_b' (leading to the maximum $\Delta Q'$) in the subsurface dam cases appears to be 0.67. These trends arise because when the subsurface dam moves away from the shoreline, the saltwater overtopping is increasingly limited, whereas when the subsurface dam is placed close to the well, overtopping is induced by high local velocities, as mentioned above (see Figures S4 and S6). Our results also indicate that, for the fully penetrating barrier cases, the barrier placed closer to the well (i.e., greater D_b') gave rise to a larger $\Delta Q'$ (dashed line, Figure 10), which is consistent with the trends illustrated in Figure 9.

Furthermore, the increasing value of D_b' leads to a nonlinear increase of $\Delta Q'$ for the fully penetrating barrier, as shown in Figure 10. Specifically, for $D_b < x_{Tn}$ (i.e., $D_b = 0$, 0.11, and 0.22), the increasing D_b' gives rise to a decreasingly growth of $\Delta Q'$, while for $D_b > x_{Tn}$ (i.e., $D_b = 0.44$, 0.67, and 0.89), the curve (of $\Delta Q'$ vs. D_b') shows the opposite trend (black dashed lines, Figure 10). The nonlinear behavior of $\Delta Q'$ for the fully penetrating barrier cases is probably determined by the relationship between the barrier and the initial toe location (i.e., D_b and x_{Tn}, respectively). As shown in Figures S5k and S5l, although the barriers placed within the initial seawater wedge (i.e., $D_b < x_{Tn}$) produce the similar toe positions within the shore-perpendicular cross section (at $y = L_b/2$), the volume of saltwater wedge on the landward side of the barrier was significantly reduced by a more landward barrier, producing a larger $\Delta Q'$. That is, the increment of $\Delta Q'$ caused by the increasing D_b can be attributed to the reduction of saltwater volume on the landward side of the barrier for $D_b < x_{Tn}$, where the increasing D_b' leads to a smaller reduction rate of the saltwater volume on the landward side of the barrier. However, for $D_b > x_{Tn}$, the barrier of a larger D_b' produces the saltwater wedge that is more landward within the shore-perpendicular cross section (at $y = L_b/2$, Figures S5m–S5o), increasingly limiting the saltwater bypassing around the vertical edge of the barrier, as expected.

Figure 10b shows that cutoff walls of greater h_b' led to larger $\Delta Q'$ for all D_b' values tested, indicating that deeper cutoff walls offer greater resistance to the underlying saltwater movement toward the well. As expected, fully penetrating barriers outperformed cutoff walls in terms of $\Delta Q'$ (Figure 10b).

Relationships between $\Delta Q'$ and D_b' for cutoff walls (Figure 10b) reveal ideal distances from the shoreline for the cases that were considered. That is, as the cutoff wall was shifted further away from the shoreline, $\Delta Q'$ first increased to a peak value and then reduced. The optimal D_b' (i.e., leading to peak values of $\Delta Q'$) values for cutoff wall cases with h_b' of 0.4, 0.6, and 0.8 were 0.11, 0.22, and 0.44, respectively, as shown in Figure 10b. It indicates that cutoff wall performance depends on the depth of the seawater wedge at the barrier location (prior to the barrier construction). That is, if saltwater can pass unimpeded through the cutoff wall opening (which increasingly occurs for larger D_b' values), or if the density effects acting to force seawater through the cutoff wall opening are large (which occurs when the barrier is near the shoreline, or small D_b' values), the effectiveness of the barrier in increasing the maximum safe pumping is reduced (as mentioned above for the nonpumping case, and as evident in $\Delta x_{Tc}'$ results of Figure 7d). The inefficiency

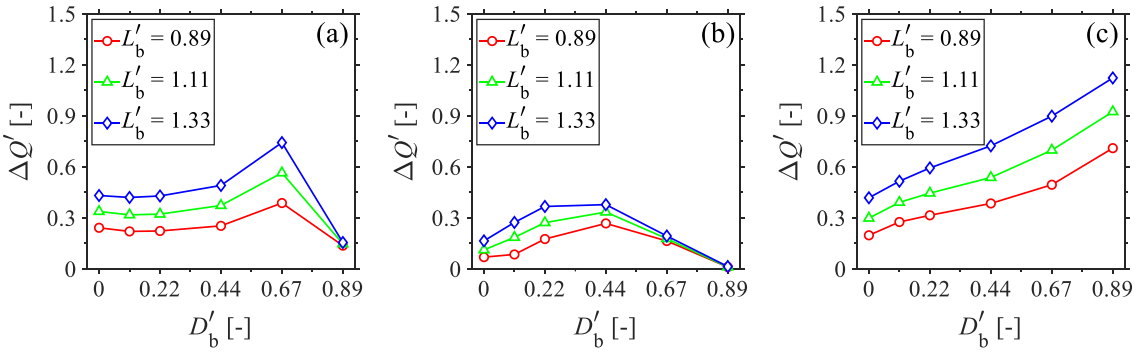

Figure 11. Sensitivity of $\Delta Q'$ to L_b' and D_b' for the case of: (a) subsurface dam, (b) cutoff wall, and (c) fully penetrating barrier, where $h_b' = 0.8$ and 1.0 for partially and fully penetrating barrier cases, respectively.

of the cutoff wall placed at $D_b' = 0.89$ is mainly because at such a distance the wall may prevent the freshwater from repulsing the saltwater, as mentioned above.

Figure 11 shows the sensitivity of $\Delta Q'$ to L_b' and D_b' for partially ($h_b' = 0.8$) and fully penetrating barrier cases. Larger L_b' values led to greater $\Delta Q'$ for each type of barrier with the same D_b'. Comparisons of flow vector and salinity distributions within the *xy* plane (the bottom layer) given in Figure S8 for different values of L_b' provide insight into the key controlling mechanisms. For example, Figure S8 shows that the performances of the subsurface dam and fully penetrating barrier were associated with the saltwater bypassing vertical barrier edges, causing slightly more landward seawater extent in areas without barrier coverage. It follows that longer barriers led to greater freshwater protection by lengthening flow paths between the well and the sea, under the action of pumping. Figure S9 shows flow vector and salinity distributions (*xy* plane; bottom layer) for cutoff wall cases of different L_b' that indicate that longer cutoff walls impeded more saltwater on the seaward side of the wall, thereby offering greater resistance to saltwater incursion and leading to higher maximum safe pumping rates.

The optimal D_b' (producing the maximum $\Delta Q'$) was 0.67 for every tested L_b' of the subsurface dam case (Figure 11a), whereas, for the cutoff wall case, the optimal D_b' was 0.44 (Figure 11b). The subsurface dam placed at $D_b' = 0.89$ obtained a dramatic decrease in performance for all tested L_b', indicating that the saltwater overtopping (over the dam crest) occurs in these cases, as mentioned above (i.e., Figure 9e). In the fully penetrating barrier cases, the largest D_b' (0.89) was the optimal value (in terms of $\Delta Q'$) for all L_b' values tested (Figure 11c). These trends are consistent with the results of the cases with $L_b' = 1.11$, as illustrated in Figure 10.

Furthermore, the results for sensitivities of $\Delta V'$, $\Delta x_{Tc}'$, and $\Delta x_{Te}'$ to different L_b' and D_b', including the subsurface dam and the cutoff wall cases with $h_b' = 0.4$ and 0.6, are incorporated into Section S4.2 and Figure S11, for the sake of brevity.

4. Discussion

Although physical barriers are commonly encountered in unconfined aquifers, Kaleris and Ziogas (2013) demonstrated that comparisons between the barrier effectiveness obtained in unconfined and confined aquifers did not show great differences in terms of seawater intrusion prevention. Systematic comparisons of the barrier performance in confined and unconfined aquifers are beyond the purpose of this study. Nonetheless, the simulations, including several barrier cases from the barrier-only and the barrier-well systems, were conducted in a corresponding unconfined aquifer (i.e., using the parameter values adopted in the confined setting of this study); the results of which are illustrated and analyzed in Section S5 and Figures S13 and S14. The results obtained in unconfined and confined aquifers indicate the similar trends (in terms of the performance of the barriers) in both barrier-only and barrier-well systems, as expected.

Optimal performance of the three barrier types in excluding seawater was obtained for different values of D_b' and h_b' (for subsurface dams and cutoff walls) and was dependent on the performance indicators

(maximum $\Delta V'$, $\Delta x_{Tc}'$, or $\Delta x_{Te}'$), as shown in Figure 6. Subsurface dams performed optimally (in terms of all three performance indicators) with larger h_b' and with $D_b' = 0.11$, except in terms of $\Delta x_{Tc}'$ for $h_b' = 0.4$, for which $D_b' = 0.22$ produced optimal performance. Cutoff walls also performed optimally for the largest values of h_b', as discussed above. However, the optimal location of cutoff walls depended on the performance indicator, whereby $\Delta V'$ and $\Delta x_{Te}'$ reached maximum values with the barrier at the shoreline ($D_b' = 0$; Figures 6b and 6f), whereas the value of D_b' producing the largest $\Delta x_{Tc}'$ was 0.11 (Figure 6d). This nuances the previous 2D investigation of Luyun et al. (2011), who found that greater reduction of the toe position (e.g., larger $\Delta x_{Tc}'$) should be achieved with cutoff walls located closer to the coast. Clearly, the component of groundwater flow parallel to the wall, which cannot be considered in 2D models, plays an important role in the ideal positioning of finite-length cutoff walls.

In previous 2D studies by Luyun et al. (2009) and Chang et al. (2019), subsurface dams that constructed with a height equal to (or slightly lower than) the thickness of the seawater wedge at the dam location (prior to dam construction), were found to be effective in limiting the landward extent of saltwater in coastal aquifers. However, our numerical results reveal that the effectiveness of finite-length subsurface dams is significantly weaker compared to a subsurface dam that considered only in a cross-sectional view of the coastal aquifer (see Figures 6 and 7). That is, seawater bypassing around the vertical edge of finite-length subsurface dams leads to significant volumes of seawater on the landward side of the barrier, although the dam is higher than the seawater wedge thickness at the barrier location (see Figures 3b and 5a).

The effectiveness of partially penetrating barriers in excluding seawater and enhancing allowable extraction has been well documented in previous studies, although few quantitative comparisons have been made between cutoff walls and subsurface dams. Our numerical results indicate that cutoff walls and subsurface dams perform better in barrier-only and barrier-well systems, respectively. This arises because in the barrier-only system, the seaward fresh groundwater flow is forced through the opening at the aquifer bottom, which acts to oppose the landward penetration of the underlying saltwater wedge, whereas freshwater flows over the crest of subsurface dams in a similar manner to the discharge of fresh groundwater in the absence of a barrier. In contrast, pumping draws saltwater toward the well primarily along the bottom of the aquifer, which is more effectively blocked by the subsurface dam compared to the cutoff wall, which has an opening at the bottom.

An important consideration in the design of finite-length barriers is the pathway of groundwater discharge to the sea around the barrier. In the case of a fully penetrating impermeable barrier, freshwater discharge to the sea is cut off entirely (in the 2D conceptual model), whereas in the finite-length case, freshwater is redirected around the barrier. Thus, finite-length fully penetrating barriers may be better suited to situations where inland soil salinization and accumulation of pollutants are expected to arise if discharge to sea is blocked (and groundwater levels rise as a consequence). Moreover, although fully penetrating barrier performs optimally among three types of barriers in most cases (for both confined and unconfined settings), it may cause greater negative effect (i.e., inland soil salinization and accumulation of pollutants) than the corresponding partially penetrating barriers, especially in unconfined settings where excessive groundwater would build up on the landward side of the barrier.

Furthermore, physical barriers constructed in the field cases may be much shorter or longer than the scenarios tested in this study, such as those reported in the Japan Green Resources Agency (2004). However, our results summarize the characteristics of the physical barrier in preventing seawater intrusion and enhancing allowable freshwater extraction in 3D aquifers, which is expected to guide the management and investigation of barrier systems in the real-world settings. For example, saltwater bypassing around the vertical edge of the barrier would be the main concern in cases involving barriers of great height but short length, whereas for long barriers with a low height, saltwater overtopping or encroachment through the opening is more likely to cause the failure of the barrier.

The choice of salinity limits may affect the results presented in this study due to the challenges of capture real-world saltwater-freshwater mixing zones in the numerical simulation of relatively simple conceptual models. For example, the choice of salinity values determines the toe position, maximum safe pumping rates and other indicators and therefore may have influenced barrier performance calculations. Nonetheless, salinity limits used in this investigation tend to be conservative, considering the purpose of providing safe

strategies for groundwater management and exploitation in coastal aquifers with the addition of the barrier. The same can be said about our choice of dispersion parameters, although we are close to the practical lower limit of dispersivity values, because cell sizes are as small as restrictions to computer run times (which were relatively long) would allow.

5. Conclusions

This study used 3D numerical modeling to quantitatively investigate the performances of three types of finite-length subsurface barriers, under both pumping and barrier-only (i.e., no pumping) situations, in limiting seawater intrusion and enhancing groundwater extraction in simplified representations of coastal confined aquifers. In barrier-only systems, optimal performance of each barrier type depended on which performance indicator (i.e., saltwater volume and seawater wedge toe position) was considered. Generally, the cutoff wall was more effective (in the absence of pumping) than subsurface dams of the same vertical dimension in terms of excluding seawater, especially for barriers close to the shoreline, and that were high and long. In all cases, a fully penetrating barrier performed optimally.

In barrier-well systems, subsurface dams of greater height or length produced larger maximum safe pumping rates when placed at the optimal location; for our model parameters, this was 300 m. Cutoff walls with larger heights or lengths also led to greater maximum safe pumping rates, where the optimal location (producing the maximum safe pumping rate) was determined by the specific values of height and length. Nonetheless, subsurface dams perform better than cutoff walls in pumping scenarios in terms of maximum safe pumping rates. Again, fully penetrating barriers with larger lengths or locations performed better.

The design of barrier systems to prevent seawater intrusion under real-world conditions likely requires consideration of additional factors to those included in the current analysis, such as aquifer heterogeneity, barrier permeability, complex boundary condition (or geometry), sea-level rise, and other temporal and spatial variations. Nevertheless, the current research, based on the typical aquifer parameters and possible barrier variables, provides a useful assessment of the effectiveness of finite-length barriers for potential applications and offers insight into barrier design parameters.

Acknowledgments

C. Lu acknowledges the financial support from the National Key Research Project (2018YFC0407200), National Natural Science Foundation of China (51679067 and 51879088), and Fundamental Research Funds for the Central Universities (B200204002). Adrian Werner is the recipient of an Australian Research Council Future Fellowship (project number FT150100403). The study is theoretical, and no data are available. The authors would like to thank Marc Walther, Antoifi Abdoulhalik, an anonymous reviewer, and editors for their valuable comments and suggestions.

References

Abdoulhalik, A., Ahmed, A., & Hamill, G. A. (2017). A new physical barrier system for seawater intrusion control. *Journal of Hydrology*, *549*, 416–427. https://doi.org/10.1016/j.jhydrol.2017.04.005

Abdoulhalik, A., & Ahmed, A. A. (2017a). The effectiveness of cutoff walls to control saltwater intrusion in multi-layered coastal aquifers: Experimental and numerical study. *Journal of Environmental Management*, *199*, 62–73. https://doi.org/10.1016/j.jenvman.2017.05.040

Abdoulhalik, A., & Ahmed, A. A. (2017b). How does layered heterogeneity affect the ability of subsurface dams to clean up coastal aquifers contaminated with seawater intrusion? *Journal of Hydrology*, *553*, 708–721. https://doi.org/10.1016/j.jhydrol.2017.08.044

Anwar, H. O. (1983). The effect of a subsurface barrier on the conservation of freshwater in coastal aquifers. *Water Research*, *17*(10), 1257–1265. https://doi.org/10.1016/0043-1354(83)90250-6

Ataie-Ashtiani, B., & Ketabchi, H. (2011). Elitist continuous ant colony optimization algorithm for optimal management of coastal aquifers. *Water Resources Management*, *25*(1), 165–190. https://doi.org/10.1007/s11269-010-9693-x

Bear, J., Cheng, A. H.-D., Sorek, S., Ouazar, D., & Herrera, I. (Eds.) (1999). *Seawater intrusion in coastal aquifers: Concepts, methods and practices* (Vol. 14, p. 591). Dordrecht, Netherlands: Springer Science and Business Media.

Chang, Q., Zheng, T., Zheng, X., Zhang, B., Sun, Q., & Walther, M. (2019). Effect of subsurface dams on saltwater intrusion and fresh groundwater discharge. *Journal of Hydrology*, *576*, 508–519. https://doi.org/10.1016/j.jhydrol.2019.06.060

Cheng, A. D., Halhal, D., Naji, A., & Ouazar, D. (2000). Pumping optimization in saltwater-intruded coastal aquifers. *Water Resources Research*, *36*(8), 2155–2165. https://doi.org/10.1029/2000WR900149

Custodio, E. (1987). *Methods to control and combat saltwater intrusion, studies and reports in hydrology: groundwater problems in coastal areas* (pp. 396–433). Paris, France: UNESCO.

Dror, I., Berkowitz, B., & Gorelick, S. M. (2004). Effects of air injection on flow through porous media: Observations and analyses of laboratory-scale processes. *Water Resources Research*, *40*, W09203. https://doi.org/10.1029/2003WR002960

Ebeling, P., Händel, F., & Walther, M. (2019). Potential of mixed hydraulic barriers to remediate seawater intrusion. *Science ot the Total Environment*, *693*. https://doi.org/10.1016/j.scitotenv.2019.07.284

Guo, W., & Langevin, C. D. (2002). User's guide to SEAWAT: A computer program for simulation of three-dimensional variable-density ground-water flow. In *U.S. Geological Survey Techniques and Methods* (p. 77). Tallahassee, FL: U.S. Geological Survey. https://doi.org/10.3133/twri06A7

Japan Green Resources Agency (2004). *Technical Reference for Effective Groundwater Development* (p. 325). Saiwai-ku, Kawasaki, Kanagawa Prefecture, Japan: Japan Green Resources Agency. Retrieved from https://www.jircas.go.jp/en/file/67536/download?token=WYgbdYBZ

Kaleris, V. K., & Ziogas, A. I. (2013). The effect of cutoff walls on saltwater intrusion and groundwater extraction in coastal aquifers. *Journal of Hydrology*, *476*, 370–383. https://doi.org/10.1016/j.jhydrol.2012.11.007

Langevin, C. D., Shoemaker, W. B., & Guo, W. (2003). *MODFLOW-2000, the U.S. Geological Survey modular ground-water model—Documentation of the SEAWAT-2000 Version with the Variable-Density Flow Process (VDF) and the Integrated MT3DMS Transport Process (IMT)* (p. 43). Tallahassee, FL: U.S. Geological Survey. https://doi.org/10.3133/ofr03426

Li, F., Chen, X., Liu, C., Lian, Y., & He, L. (2018). Laboratory tests and numerical simulations on the impact of subsurface barriers to saltwater intrusion. *Natural Hazards*, *91*(3), 1223–1235. https://doi.org/10.1007/s11069-018-3176-4

Lu, C., Shi, W., Xin, P., Wu, J., & Werner, A. D. (2017). Replenishing an unconfined coastal aquifer to control seawater intrusion: Injection or infiltration? *Water Resources Research*, *53*, 4775–4786. https://doi.org/10.1002/2016WR019625

Lu, C., & Werner, A. D. (2013). Timescales of seawater intrusion and retreat. *Advances in Water Resources*, *59*, 39–51. https://doi.org/10.1016/j.advwatres.2013.05.005

Lu, C., Werner, A. D., Simmons, C. T., Robinson, N. I., & Luo, J. (2013). Maximizing net extraction using an injection-extraction well pair in a coastal aquifer. *Groundwater*, *51*(2), 219–228. https://doi.org/10.1111/j.1745-6584.2012.00973.x

Lu, C., Xin, P., Li, L., & Luo, J. (2015). Steady state analytical solutions for pumping in a fully bounded rectangular aquifer. *Water Resources Research*, *51*, 8294–8302. https://doi.org/10.1002/2015WR017019

Luyun, R., Momii, K., & Nakagawa, K. (2009). Laboratory-scale saltwater behavior due to subsurface cutoff wall. *Journal of Hydrology*, *377*(3–4), 227–236. https://doi.org/10.1016/j.jhydrol.2009.08.019

Luyun, R., Momii, K., & Nakagawa, K. (2011). Effects of recharge wells and flow barriers on seawater intrusion. *Groundwater*, *49*(2), 239–249. https://doi.org/10.1111/j.1745-6584.2010.00719.x

Mahesha, A. (1996a). Control of seawater intrusion through injection-extraction well system. *Journal of Irrigation and Drainage Engineering*, *122*(5), 314–317. https://doi.org/10.1061/(ASCE)0733-9437(1996)122:5(314)

Mahesha, A. (1996b). Steady-state effect of freshwater injection on seawater intrusion. *Journal of Irrigation and Drainage Engineering*, *122*(3), 149–154. https://doi.org/10.1061/(ASCE)0733-9437(1996)122:3(149)

Mahesha, A. (1996c). Transient effect of battery of injection wells on seawater intrusion. *Journal of Hydraulic Engineering*, *122*(5), 266–271. https://doi.org/10.1061/(ASCE)0733-9429(1996)122:5(266)

Mahesha, A. (2009). Conceptual model for the safe withdrawal of freshwater from coastal aquifers. *Journal of Environmental Engineering*, *135*(10), 980–988. https://doi.org/10.1061/(ASCE)EE.1943-7870.0000081

Mahesha, A., & Lakshmikant, P. (2014). Saltwater intrusion in coastal aquifers subjected to freshwater pumping. *Journal of Hydrologic Engineering*, *19*(2), 448–456. https://doi.org/10.1061/(asce)he.1943-5584.0000789

Mantoglou, A. (2003). Pumping management of coastal aquifers using analytical models of saltwater intrusion. *Water Resources Research*, *39*(12), 1335. https://doi.org/10.1029/2002WR001891

Masciopinto, C. (2013). Management of aquifer recharge in Lebanon by removing seawater intrusion from coastal aquifers. *Journal of Environmental Management*, *130*, 306–312. https://doi.org/10.1016/j.jenvman.2013.08.021

Michael, H. A., Post, V. E., Wilson, A. M., & Werner, A. D. (2017). Science, society, and the coastal groundwater squeeze. *Water Resources Research*, *53*, 2610–2617. https://doi.org/10.1002/2017WR020851

Oude Essink, G. H. (2001). Improving fresh groundwater supply—Problems and solutions. *Ocean and Coastal Management*, *44*(5–6), 429–449. https://doi.org/10.1016/S0964-5691(01)00057-6

Pool, M., & Carrera, J. (2010). Dynamics of negative hydraulic barriers to prevent seawater intrusion. *Hydrogeology Journal*, *18*(1), 95–105. https://doi.org/10.1007/s10040-009-0516-1

Pool, M., & Carrera, J. (2011). A correction factor to account for mixing in Ghyben-Herzberg and critical pumping rate approximations of seawater intrusion in coastal aquifers. *Water Resources Research*, *47*, 143–158. https://doi.org/10.1029/2010WR010256

Post, V. E. A., Bosserelle, A. L., Galvis, S. C., Sinclair, P. J., & Werner, A. D. (2018). On the resilience of small-island freshwater lenses: Evidence of the long-term impacts of groundwater abstraction on Bonriki Island, Kiribati. *Journal of Hydrology*, *564*, 133–148. https://doi.org/10.1016/j.jhydrol.2018.06.015

Sugio, S., Nakada, K., & Urish, D. W. (1987). Subsurface seawater intrusion barrier analysis. *Journal of Hydraulic Engineering*, *113*(6), 767–779. https://doi.org/10.1061/(ASCE)0733-9429(1987)113:6(767)

Sun, D. M., & Semprich, S. (2013). Using compressed air injection to control seawater intrusion in a confined coastal aquifer. *Transport in Porous Media*, *100*(2), 259–278. https://doi.org/10.1007/s11242-013-0215-1

Werner, A. D. (2010). A review of seawater intrusion and its management in Australia. *Hydrogeology Journal*, *18*(1), 281–285. https://doi.org/10.1007/s10040-009-0465-8

Werner, A. D., Bakker, M., Post, V. E. A., Vandenbohede, A., Lu, C., Ataie-Ashtiani, B., et al. (2013). Seawater intrusion processes, investigation and management: Recent advances and future challenges. *Advances in Water Resources*, *51*, 3–26. https://doi.org/10.1016/j.advwatres.2012.03.004

Zheng, C., & Bennett, G. D. (2002). *Applied contaminant transport modeling* (2nd ed. pp. 184–187). New York: Wiley-Interscience.

Zheng, C., & Wang, P. P. (1999). *MT3DMS: A modular three-dimensional multispecies transport model for simulation of advection, dispersion and chemical reactions of contaminants in groundwater systems: Documentation and user's guide, Contract Report SERDP-99-1*. Vicksburg, MS: U.S. Army Corps of Engineers-Engineer Research and Development Center.